

# Excitation energy transfer in conjugated polymer/silicon nanocrystal-based bulk heterojunctions\*

Vladimir Švrček†

Research Center for Photovoltaics, National Institute of Advanced Industrial Science and Technology (AIST), Tsukuba, Japan

**Abstract:** An excitation energy transfer in a bulk heterojunction based on freestanding silicon nanocrystals (Si-NCs) and conjugated polymers {poly(3-hexylthiophene) (P3HT), poly[2-methoxy-5-(2-ethyl-hexyloxy)-1,4-phenylene vinylene] (MEH-PPV)} is demonstrated. The electrochemical etching process is employed for fabrication of freestanding and polymer soluble Si-NCs. Formation of a bulk heterojunction is confirmed by a difference in a work function of both polymers and an ionization potential of the NCs. An annealing step significantly influences the polymer chain conformation and electronic interaction between the polymer and the NC, which improves the exciton energy migration. The presence of the Si-NCs in polymers suppresses the relative intensity of vibronic peaks, resulting in a red-shift of the blend photoluminescence (PL) spectra. This phenomenon is attributed to a temperature-dependent migration process of singlet exciton and Dexter excitation energy transfer from the polymer to the NC. Compared to MEH-PPV polymer, a lamella-type stacking structure of the P3HT and an abridged PL spectra overlap with NCs decreases an excitation energy transfer rate. At the same time, an improvement in photocurrent generation is recorded when Si-NCs are embedded in P3HT polymer. After Dexter-like excitonic energy transfer, the PL emission of both blends is controlled through a quantum confinement effect and electron-hole recombination in Si-NCs.

**Keywords:** excitation energy transfer; conjugated polymers; photoconductivity; photoluminescence; silicon nanocrystals.

## INTRODUCTION

Although the early proof-of-principle work on organic photovoltaics in the mid-1980s was demonstrated, the organic photovoltaic devices are still in a comparatively early stage of development [1]. Meanwhile, poly(phenylene vinylene) (PPV) and poly(thiophene) derivatives, as electron-donating conjugated polymers, have been widely investigated [2,3]. Due to the better chemical stability, higher carrier mobility, and lower optical bandgap [4,5], better photovoltaic performances have been obtained in poly(thiophene) rather than in PPV derivatives [6]. The importance of silicon in the photovoltaics industry has led to the design and investigation of many kinds of hybrid Si/conjugated-polymer-based devices [7,8]. In order to improve a device performance, tuning of the interaction between bulk silicon and polymers by solvent and/or by temperature annealing treatments has been widely reported in the liter-

\*Paper based on a presentation at the 5<sup>th</sup> International Symposium on Novel Materials and Their Synthesis (NMS-V) and the 19<sup>th</sup> International Symposium on Fine Chemistry and Functional Polymers (FCFP-XIX), 18–22 October 2009, Shanghai, China. Other presentations are published in this issue, pp. 1975–2229.

†E-mail: vladimir.svrek@nist.go.jp

ature [9,10]. However, existing polymer-based solar cells so far do not convert solar energy into electricity as efficiently as they could and an improvement in conversion efficiency is needed [6,11–13]. One way to improve device efficiency is blending of the polymer with a second nanocomposite structure [14–17]. A donor–acceptor bulk heterojunction using semiconducting polymers and fullerene is currently the most commonly used approach [18], and an improved photovoltaic performance is mostly attributed to the great electron acceptability of the fullerene [1,6].

In order to improve the photovoltaic performance, it is crucial to understand the various loss mechanisms so that these may be overcome by a better material design. In general, for a donor–acceptor bulk heterojunction to be a feasible system, at least two important conditions must be fulfilled: (i) electronic transport efficiency must be increased by balancing carrier distribution and minimizing loss through the charge trapping and recombination [19–22], and (ii) optical absorption must overlap as much of the solar spectrum as possible [23,24]. In order to enable more productive solar energy conversion, the semiconductor nanocrystals (quantum dots) are being extensively explored [20,25–27]. However, freestanding silicon nanocrystals (Si-NCs) [27] offer an improvement in several of key aspects: First of all, the electron affinity of silicon (3.9 eV) is larger than fullerene (2.6 eV), which may increase the probability of charge separation [27]. Then, the spectral absorption coverage can be simply adjusted since in the quantum regime (i.e., Si-NC size smaller than 10 nm) Si-NCs tunable broad band absorption [28]. After that, an excited-state lifetime is rather long, thus increasing the probability of photoexcited excitons being swept away by the inbuilt electric field. Next, the minority carrier multiplication discovered in Si-NCs [29] can significantly boost the photocurrent generations, and finally, nontoxicity for the environment [30] might bring considerable benefit for sustainable hybrid solar cell development. It is assumed that a combination of those properties makes freestanding Si-NCs an attractive material and optically active component when blended with conjugated polymers [27].

In this paper, the optoelectronic properties of two optically active components based on blending Si-NCs with conjugated polymers {poly(3-hexylthiophene) (P3HT) and poly[2-methoxy-5-(2-ethylhexyloxy)-1,4-phenylene vinylene] (MEH-PPV)} are shown. Blending of Si-NCs with chosen polymers leads to formation of a bulk heterojunction. A larger ratio between photo- and dark-conductivity is observed in the case of a lamella-type stacking P3HT polymer-based blend. Contrary to pure polymer films, the presence of Si-NCs in both polymers leads to a red-shift of PL emission spectra as a result of the Dexter excitation energy transfer from the polymer to the NC.

## EXPERIMENTAL

As described elsewhere [31], the freestanding Si-NCs in this work were fabricated by electrochemical etching of crystalline Si wafers and harvested by mechanical scratching. Namely, phosphorus-doped wafers with a resistivity of 0.5–2 Ω·cm (n-type, <100>, P concentration  $\sim 2 \times 10^{16} \text{ cm}^{-3}$ ) were used. The wafers were electrochemically etched in a mixture of hydrofluoric acid with pure ethanol (HF:C<sub>2</sub>H<sub>5</sub>OH = 1:4) at a current density at 1.6 mA/cm<sup>2</sup>. Etching time was 90 min, and a halogen lamp illuminated a Si substrate during the electrochemical etching. Since the Si-NC powder is obtained by mechanical pulverization of porous Si thin films [31], large micrograins are also present in the powder. The largest micrograins can be eliminated by sedimentation and filtration [31,32]. In our case, the largest micrograins were eliminated by sedimentation of the powder in ethanol solution for 30 min. Then, a supernatant colloidal solution was dried and Si-NC powder were used for fabrication of the blends. The scanning electron microscopy (SEM) observations show that the Si-NC powder even after sedimentation contains Si-NC grains (clusters) of several μm (see Fig. 1a). Systematic studies of high-resolution transmission electron microscopy (HR-TEM) [31] and single quantum dot spectroscopy [32] observations showed that such a powder contains both single Si-NCs and Si-NC micrograins. Si-NC micrograins consist of many NCs (ranging from about 2 to 6 nm) interconnected and kept together by amorphous tissue, e.g., SiO [31,32]. In this work, we have used micro-Raman and photoluminescence (PL) spectroscopy to check the presence of the Si-NCs in the powder. Corresponding Raman spectra of

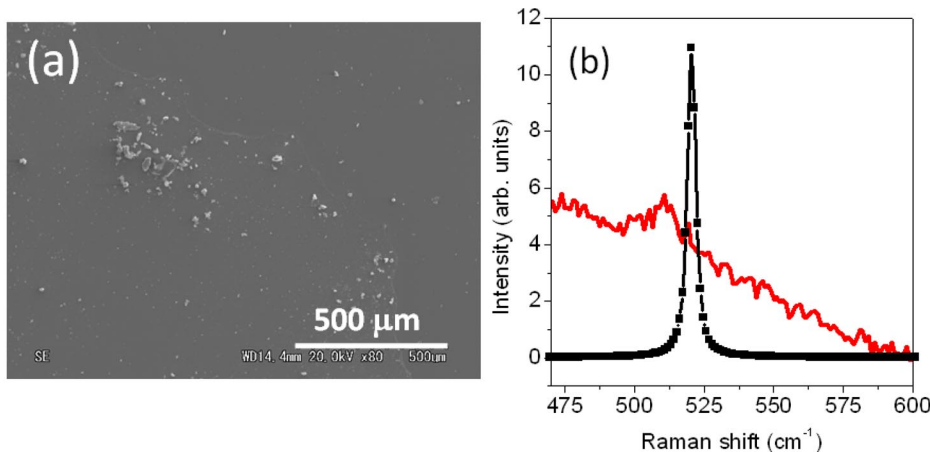


**Fig. 1** (a) SEM image of Si-NC powder prepared by electrochemical etching dispersed on quartz substrate. (b) Red curve represents corresponding Raman spectrum of Si-NC powder dispersed on quartz substrate. Black symbol line shows a spectrum of a Si wafer used for fabrication of Si-NCs and is shown for comparison.

dispersed Si-NC powder on a quartz substrate is shown in Fig. 1b (red line). Compared to that of crystalline Si (black symbol line) the spectrum of the Si-NC powder exhibits a peak shift maxima of about  $\sim 11\text{ cm}^{-1}$  and spectra broadening with peak widths of  $\sim 22\text{ cm}^{-1}$ . According to ref. [33], the corresponding Si-NC size of about  $\sim 3\text{ nm}$  on average was evaluated.

Then, both commercially available (Aldrich) polymers P3HT and MEH-PPV were dissolved in chlorobenzene. The blends were prepared by dissolving 10 mg of polymer in 10 g of chlorobenzene. The 400 mg of polymer solution and 2 mg of Si-NC were mixed to make the films. For the photoconductivity measurements, 300-nm thin films were spun cast on a Si substrate and on a glass covered by interdigitated platinum contact (20 fingers, with a length of 6 mm and a width of 200  $\mu\text{m}$ ). With the same conditions, another set of samples with pure polymers (MEH-PPV, P3HT) was fabricated for comparison. For all cases, the samples were annealed at 415 K for 30 min in a vacuum.

The conductivity and the PL measurements were conducted in air or vacuum atmosphere, respectively. A voltage from a regulated DC power supply was applied, and the resulting current was measured with an amperometer (Sub Femtoamp, KEITHLEY 6430). For photoconductivity measurement, a white light of 1.5 AM was used. To measure temperature-dependent PL, the samples were placed in He-cooled cryostat where the temperature varied from 4 to 300 K. An excitation was conducted by a HeCd laser with a wavelength of 325 nm (3.82 eV).

## RESULTS AND DISCUSSION

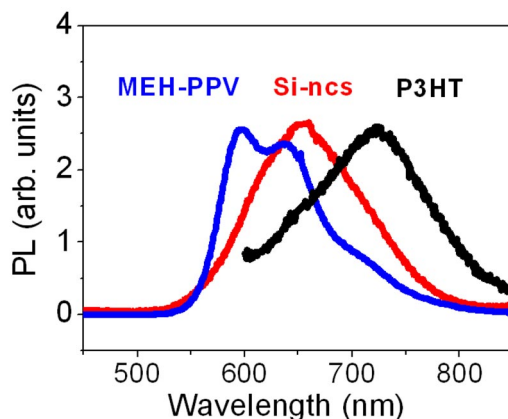
### Si-NC/polymer bulk heterojunction

Figure 2 shows room-temperature PL spectra of Si-NCs (red line) and pure-conjugated polymer (P3HT, black line; MEH-PPV, blue line) films. A significant broad red-luminescent band from freestanding Si-NCs is recorded. It is well known that when the Si grain size decreases to the nanoscale range ( $<10\text{ nm}$ ), at which quantum confinement effect begins to be dominant, visible PL appears at room temperature [34,35]. It is reported that there are mainly two PL emission bands in Si nanostructures with quantum confinement size.

- i) A PL band that shows a slow decay ( $\mu\text{s}$  to  $\text{ms}$ ) [36] where the confinement effect causes an enlargement of the bandgap and enhancement of PL efficiency. This band is mostly located in the red part of the spectral region (600–900 nm) [37]. We assume that the observed broad PL spec-

trum in the spectral band from 550 to 800 nm (red line, Fig. 2) with maxima at 650 nm (Fig. 2, red line) is similar in origin [38,39]. Then the broad spectrum results from the quantum confinement effect in nanocrystals with large size distribution with an average of 3 nm [31,38,39], which also corroborates quite well with the average size estimated from the micro-Raman analysis (Fig. 1b).

- ii) A fast nanosecond blue-green PL band originating predominantly from rapidly oxidized Si nanostructures [34,35,40,41] is not observed in our samples at room temperature (300 K). This is most likely due to NC relaxation in an organic-based suspension during the fabrication process when NCs were cleaned and dispersed in ethanol after electrochemical etching. A termination of free Si bonds by OH groups occurred [42], which most likely inhibited the rapid oxidation of the NC surface [41].



**Fig. 2** PL spectra measured at room temperature (300 K). Blue line recorded for pure P3HT polymer and black line for MEH-PPV polymer film. The red line represents PL from Si-NC powder. The polymer films were annealed at 415 K in vacuum. All samples are excited at 325 nm wavelength.

Indeed, as the MEH-PPV polymer emits in the spectral region from 530 to 800 nm (blue line, Fig. 2) and P3HT polymer from 600 to 850 nm (black line) a significant portion of the spectra which overlaps with NCs can be observed. In the case of MEH-PPV polymer, three typical PL sub-bands correlated to zero-phonon transition (~600 nm) and two phonon replicas (670 and 740 nm) are observed [43]. Contrary to that, the PL spectrum of the pure P3HT film does not show any particular sub-band structures. A broad PL spectrum with maximum at 730 nm is measured at room temperature (Fig. 2, black line). The wavelength of PL maxima is commonly used to estimate a degree of conjugation in the polymers [44,45]. An increase in the degree of conjugation in P3HT polymer causes a red-shift (~100 nm) of the PL spectrum. Then the PL intensity is determined by the number of excitons that undergo radiative recombination. A pronounced red-shift can be explained by preferential emission from the most extensively conjugated segments in the P3HT polymer [46].

To add to those peculiar PL properties, both polymers are good hole conductors [1]. Particularly, electronic interactions and the device performance appear to be highly affected by thermal annealing [47,48]. One can expect similar effects when Si-NCs are blended with conjugated polymers. An influence of the annealing treatment on pure and blends is summarized in Fig. 3. An improvement in transport properties of the films is recorded after an annealing step. Black lines (symbol lines) represent a dark conductivity and red (green) line conductivity of the films under AM 1.5 illumination. However, even after annealing, the charge separation and photocurrent generation in pure polymers did not occur (Fig. 3a). This is changed when the Si-NCs are added in the polymers. Then, generation of the photocurrent is observed. Figures 3b,c plot typical *I*-*V* characteristics of the Si-NC/MEH-PPV and

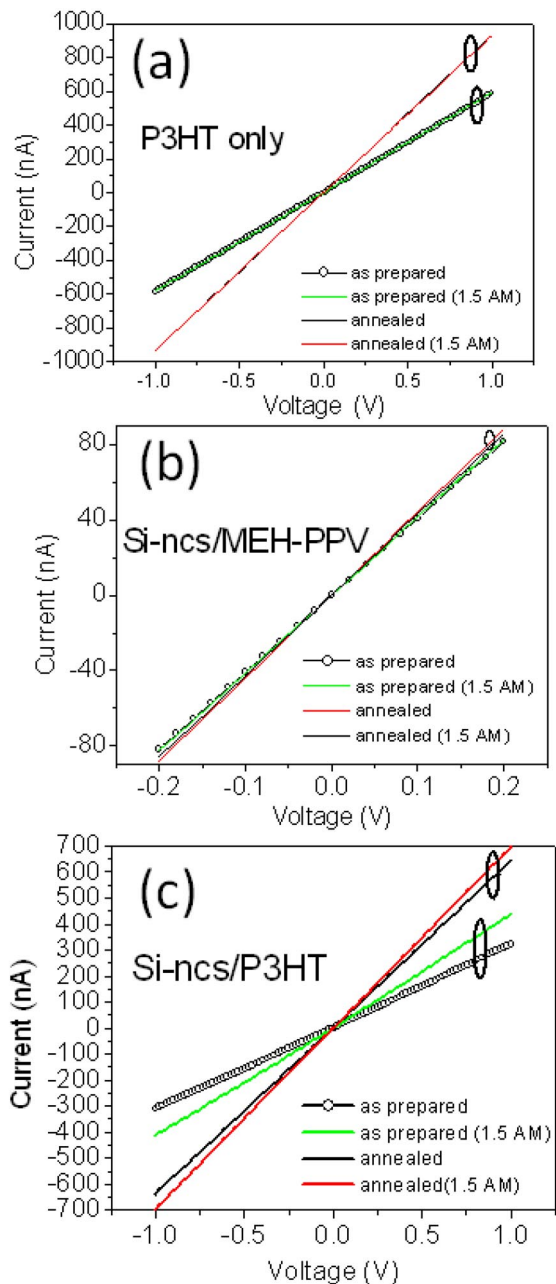


**Fig. 3** (a)  $I$ - $V$  characteristics for pure P3HT polymer film before and after annealing at 415 K are shown. (b) and (c)  $I$ - $V$  characteristics for Si-NC/MEH-PPV and Si-NC/P3HT polymer blend before and after annealing step in vacuum are plotted, respectively. Black lines/(black symbol lines) are measured in dark and red/(green) lines under AM 1.5 illumination, respectively.

Si-NC/P3HT blend before and after annealing in vacuum. It is observed that not only an increase in a dark conductivity but also an increase in generation of photocurrent occurred. Green lines represent photoconductivity before and red lines after the annealing step, respectively.

It is well known that an annealing step modifies the morphology of the polymer [40]. It is expected that an improvement of the blend morphology then considerably facilitates a charge conduction within the film. Indeed, the thermal treatment is expected to crucially affect the interface between Si-NC and polymer. As the NC decreases in size, its surface starts to play a dominant role over the bulk characteristics. Therefore, compared to the bulk Si an improvement in an interface adhesion could be more important and beneficial for blend performance. The annealing makes the polymer chains mobile, which enhances the adhesion of the interface by promoting Si–C covalent bond formation. Thus, making the effective area for electron injection larger and more current can be generated from an un-annealed one. Both polymers have similar band structures. The highest occupied molecular orbital (HOMO) is at the same level (~5 eV), and the lowest unoccupied molecular orbital (LUMO) level is at ~2.9 eV [27,49]. On the other hand, the Si-NCs have a large bandgap (~2 eV, Fig. 1) and work function around –4.1 eV. The resulting electronic interaction of NC with the polymer leads to the bulk heterojunction formation [27]. A difference in work function and ionization potentially results in an electron-hole separation and photocurrent generation under illumination (AM 1.5). Bulk heterojunction separates excitons by sweeping the holes into polymer and the electrons into NC. Due to the interfacial layer formed by interaction between the polymer and NC, a lowering of the effective injection barrier [50] is expected. In addition, it has been recently pointed out that the annealing process may lead to a more spatial exciton separation [51]. All together when acting at the same time this facilitates the exciton dissociation into free charge carriers and photocurrent generation in Si-NC/MEH-PPV,P3HT-based blends.

Figure 4a represents  $I$ – $V$  for Si-NC/MEH-PPV, and Fig. 4b shows  $I$ – $V$  of Si-NC/P3HT blend after annealing. One can observe that an electronic interaction between the NC and both polymers results in the generation of the photocurrent under illumination. It is observed that the photo-response is more important when the NCs are embedded in P3HT polymer matrix (Fig. 4b). The reasons for this are multiple. It is believed that the most important factor is the polymer structure. Figure 4 compares the chemical structure of (a) MEH-PPV and (b) P3HT polymer. On one side, the MEH-PPV derivative contains the side group (OR) onto the main chain (Fig. 5a), which facilitates its dissolution in solvent. A relatively weak 600-nm band PL intensity (Fig. 2, blue line) indicates that the polymer aggregation in chlorobenzene is quite low [43], and sufficiently high dissolution is achieved during the blending process. On the other hand, the P3HT lamella-type stacking of the side chains and thiophene rings (Fig. 5b) leads to a strong interchain interaction [52], which is apparently different from those of the MEH-PPV derivative. In this case, the blend phase separation is increased [53]. Then, it gives rise to larger, regular domain formation, which improves the transport properties through the blend [54]. As previously demonstrated by Quist et al. [55], blend morphology and domain sizes are critical for transport and device performance. Similar mechanisms are likely to affect the P3HT-based blend properties. Namely, larger regular domains by reducing the exciton recombination through an improvement of exciton diffusion while exciton dissociation should not be affected [55]. This then may lead to an increase of the photocurrent generation. Since charge carriers are not confined by the energy offsets of the polymer, an increase in a delocalization of the charge carriers can be expected [53]. Despite an exciton dissociation, an efficient charge transport in polymer blend is a serious limitation. It is well known that the P3HT also possesses higher (hole) mobility of ( $0.1 \text{ cm}^2 \text{ V}^{-1} \text{ s}^{-1}$ ) [56,57]. The lamella stacking of the side chains and thiophene rings (Fig. 5b), in addition, facilitates overall charge transport within Si-NC/P3HT blend. On the other hand, more than 5 times PL emission intensity decreased in the P3HT-based blend, which indicates that a delocalization of the charge carriers is decreased. Compared to the Si-NC/MEH-PPV film, this suggests that the photocurrent generation is less affected by the generation of free charge carriers [53].

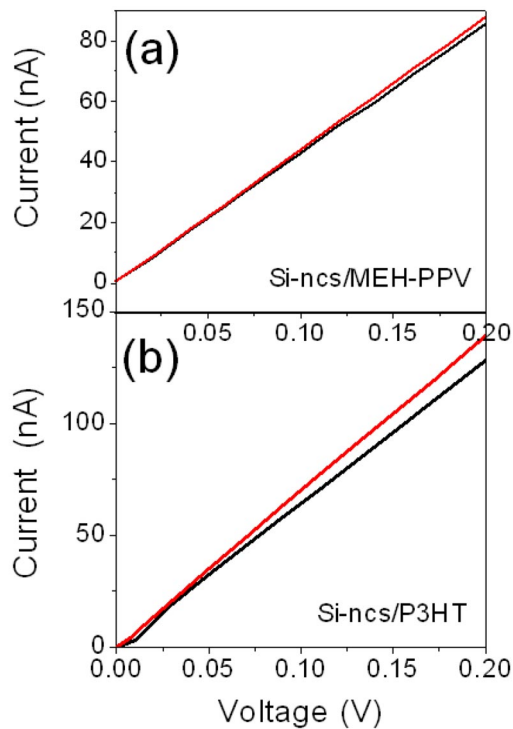


**Fig. 4**  $I$ - $V$  curves for Si-NC/polymer blends containing of Si-NCs after annealing at 415 K. Plot (a) shows the  $I$ - $V$  characteristics of MEH-PPV and (b) of P3HT polymer-based blend, respectively. Black lines are measured in dark and red lines under AM 1.5 illumination.

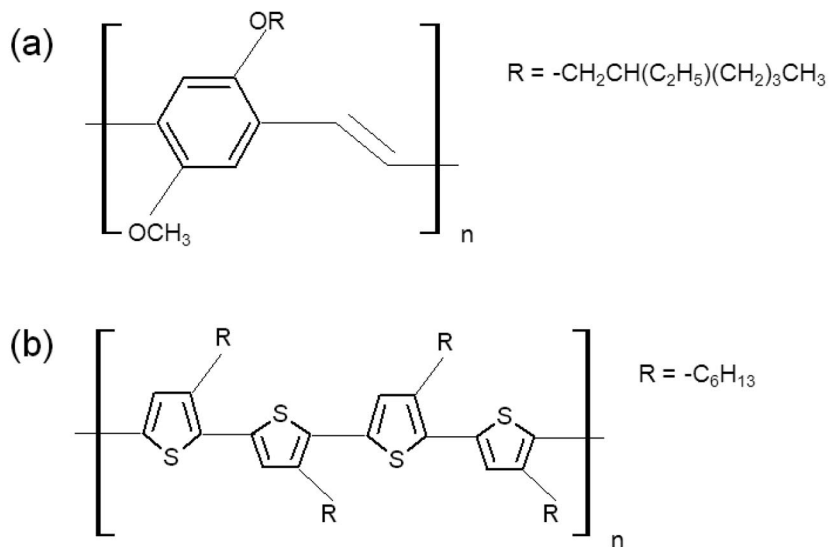


**Fig. 5** Chemical structure of (a) MEH-PPV and (b) P3HT molecule.

### Temperature-dependent PL

In order to understand the blends emission origins, let's first investigate a temperature-dependent PL of pure polymer films only. Figure 6a represents the PL spectra obtained from pure MEH-PPV polymer film and Fig. 6b from pure P3HT film at few selected temperatures. It has to be noted that the P3HT films showed lower PL intensity (~2 times) compared to MEH-PPV films. Furthermore, we observe a vibronic progression in the PL emission as a function of the temperature, which results in a blue-shift of the emission bands. The progression is rather similar for both polymers. Figure 6c summarizes the PL maxima peak shift as a function of temperature. In the case of the MEH-PPV film, two emission maximum peaks are plotted. Namely, PL vibronic peak corresponding to a zero-phonon transition (squares) and phonon-replica (triangles), respectively. The shift for both polymers reaches about 30 nm

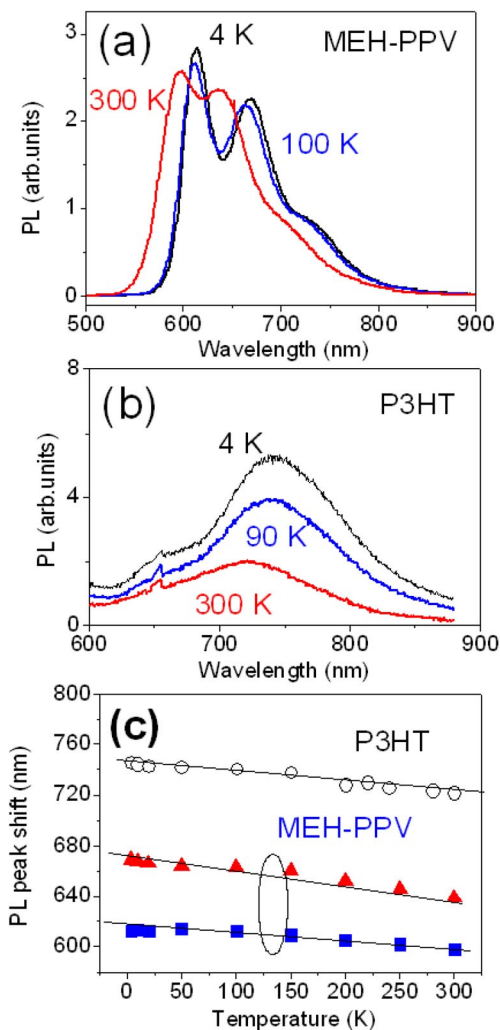


**Fig. 6** (a) PL spectra measured for (a) pure MEH-PPV polymer and (b) P3HT polymer film under excitation at 325 nm. The PL spectra taken at various temperatures are shown. (c) Summary of PL maxima peak shift as a function of the temperature for pure P3HT (circles) and MEH-PPV films is shown, respectively. The squares correspond to zero-phonon transition and triangles represent phonon-replica of PL maxima peaks in MEH-PPV polymer film.

in a temperature range from 4 to 300 K. The blue-shift indicates that in both polymers a coupling of the backbone carbon–carbon stretch vibration to electronic transitions occurred. Nevertheless, in the case of the MEH-PPV polymer two vibronic peaks not only do a blue-shift, but the relative peak intensities vary as well as a function of the temperature. The relative strength of the 600-nm peak decreases compared to the 670-nm band (Fig. 6a). This behavior in the shape of the PL spectrum has been reported previously and interpreted in terms of a decreased Huang–Rhys factor for high-frequency modes at low temperature [58,59]. A decrease of the Huang–Rhys factor results in an increase of conjugation and exciton delocalization, which is most likely made by the freezing of molecular torsions and other low-frequency emission modes.

The PL spectral features of the polymers are changed when blended with Si-NCs. Figure 7a represents PL spectra of the Si-NC/MEH-PPV polymer blend taken at 4, 50, and 300 K. The NC's PL embedded in P3HT polymer is taken at the same temperatures, shown in Fig. 7b for comparison. Contrary to the pure-polymer films, both blends show one red-shifted emission band located between 500 and 800 nm. In the presence of NCs, the quenching of PL intensity by more than 2 times is observed for

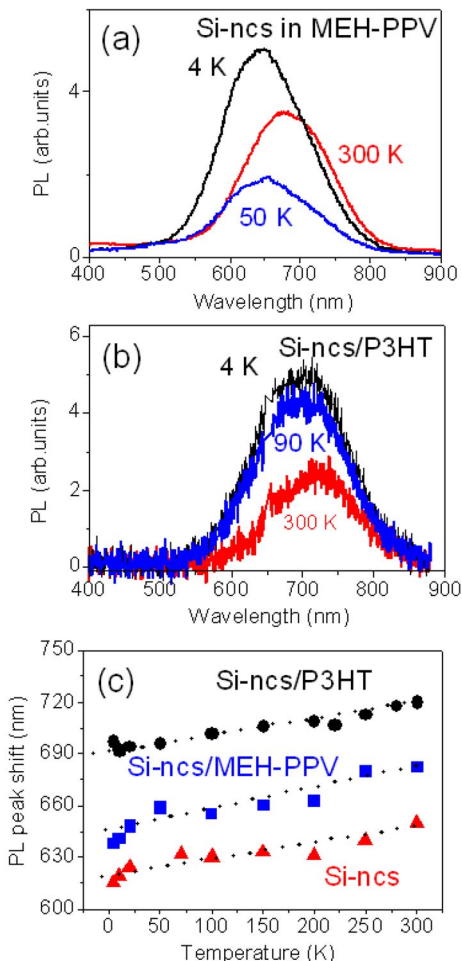


**Fig. 7** PL spectra measured for Si-NCs in (a) MEH-PPV and (b) P3HT polymer blend under excitation at 325 nm at a few selected temperatures. (c) Corresponding PL maxima peak shift taken at various temperatures for Si-NCs blended in MEH-PPV (squares) and P3HT (circles) polymer, respectively. The peak shift maxima of freestanding Si-NCs only (triangles) is shown for comparison.

both polymers. An increase in PL intensity (~5 times) in the case of the MEH-PPV blending (Fig. 7a) is due to several aspects that act at the same time. First of all, it is assumed that a lower PL intensity of pure P3HT film itself and more efficient exciton dissociation results in more important (~5 times) PL intensity quenching when Si-NCs are blended in P3HT polymer (Fig. 7b). In addition, the NC getting relaxed in a colloidal suspension and consequently the Si=O bonds, are replaced by ordinary Si–O–Si or Si–OH bonds. Then, as mentioned above, the carbon chains of polymer may take part in a passivation of the surface bonds of NCs as well [42]. Particularly in MEH-PPV polymer, the OR group (Fig. 5a) is easily soluble. After that occurrence, higher PL emission can be explained by an increased NC surface passivation. The traps become ineffective, and a radiative recombination of electron-hole pairs in the core of the NC is less affected. At the same time the generation of photocurrent is smaller, it is expected that exciplex emission is less affected and higher emission efficiency is observed in Si-NC/MEH-PPV blends.

It should be noted that embedding Si-NCs in both polymers changes the PL characteristics. Contrary to pure polymer films, red-shift of the PL band as a function of the temperature is observed (Fig. 6). Within the blends, the PL emission of the short wavelengths exhibits different temperature dependence to that of the long wavelengths. The PL behavior of both blends is rather similar to as-prepared freestanding Si-NCs (Fig. 7, triangles). However, compared to them the PL spectra are shifted and placed in a longer-wavelength spectral region. This effect is more important in the case of the P3HT-based blend and a red-shift reaching a value of about 70 nm. The summary of temperature-dependent PL maximum peaks shift is shown in Fig. 7c. It has to be noted that very similar PL behavior as a function of the temperature was previously observed for Si-NCs with quantum confinement size effect prepared by other techniques [60,61]. Therefore, the same arguments could be used here to explain our results. Due to the state filling effect, an increase in temperature decreases more strongly the emission intensity on the short wavelength side than that on the longer ones [60]. The filling effect in blended and freestanding Si-NCs leads then to a ~40-nm red-shift of PL spectrum maxima in temperature range from 4 to 300 K.

### Excitation energy transfer

The characteristics described above suggest that the PL of embedded nanocrystals in a polymer is clearly connected with quantum confinement size effects in Si-NCs. The blending of a few types of NCs in an organic matrix and the energy transfer has been investigated both theoretically and experimentally [16]. As reported elsewhere, the Förster resonance energy transfer process is one of the most important mechanisms at the nanoscale for transportation of excitation energy [63,64]. When nanocrystals are capped by an organic layer (ligands) the excitation transfer is dominated by the Förster mechanism, then the transfer is through space [65] and attributed to a dipole–dipole coupling process [66,67]. However, in our case, during the preparation process the Si-NC surface is not functionalized by any surfactant (i.e., ligands), which limits dipole–dipole coupling [65]. In addition, a dielectric constant in Si-NCs (~3 nm) is strongly confined due to quantum confinement size effects, which leads to an increased Förster transfer time from the polymer to the NC [68]. Contrary to that, when the NC does not contain any ligand groups and acceptor–donor pairs are in close distance, the excitation transfer is dominated by the Dexter mechanism, which is a charge exchange process [49,69]. In the Dexter mechanism, the spectral overlap is independent of the oscillator strength of the transitions and is efficient at very small distances [70]. An energy transfer by this mechanism requires close proximity (<10 Å) of the donor and acceptors in order to allow overlap of their wave functions [70]. We assume that in our case the donor and acceptors are in direct contact or at least in van der Waals contact. Hence, one can expect that the Dexter energy transfer may play a major role in excitation energy transfer [69,71].

The Dexter energy transfer rate ( $R_{ET}$ ) between a donor–acceptor pair at a distance ( $d$ ) can be written as follows:

$$R_{\text{ET}}(d) = \frac{2\pi}{\hbar\Psi^2} \int P_D(E)A_A(E)dE \quad (1)$$

where  $P_D(E)$  is donor emission and  $A_A(E)$  is acceptor absorption, respectively. The integral of the products is the energy conservation requirement. The  $\Psi^2$  is the exchange integral and can be expressed as follows in an asymptotic form:

$$\Psi^2 = C^2 \exp\left(-\frac{2d}{\mu_B}\right) \quad (2)$$

where  $C$  is a constant with the dimension of energy and  $\mu_B$  is the Bohr radius; in the case of Si-NCs is approximately  $\mu_B = 10$  nm and, in general, measures the spatial extent of the acceptor (NC) wave function.

As can be seen from Fig. 2a, considerable overlap between the emission of both polymers and Si-NCs is detected. A larger overlap is observed in the case of the MEH-PPV film (blue line) located, in addition, at the higher-energy spectral region. Then the exciton emission situated at lower wavelengths transfers higher excitation energies into smaller Si-NCs in diameter. Those energies are then accessible for transition into Si-NCs with a wider energy bandgap, which has more efficient emission rates [32]. As a result, a stronger emission in Si-NC/MEH-PPV compared to P3HT film is recorded (Fig. 7a). In Fig. 8, an energy band diagram for our system is proposed. The emission peak that corresponds to the lowest excited exciton energy of both polymers is around 2 eV [28,54]. Contrary to that, the exact position of ionization potential for Si-NCs is not known yet. Here we assume that the potential position does not vary significantly from a bulk Si ( $-4$  eV) [27]. The lowest exciton energy of the as-prepared Si-NCs, evaluated from PL and Raman spectroscopy, is approximately  $\sim 2$  eV (energy gap in the bulk silicon is 1.1 eV). A difference in a work function of the polymer and ionization potential of the NCs results in a band offset. If the anisotropy is included in Si-NCs as well as the dipole–dipole coupling, then it becomes easier to find a specific exciton lower energy state in the Si-NCs. When the anisotropy of the band structure is introduced, the NC's energy levels are shifted. The states become denser due to the degeneration splitting, and many optically forbidden transitions are then accessible [72]. Therefore, one may consider several states around 2 eV that appear with an inclusion of the anisotropy in the band structure of the Si-NC. Forbidden transitions around the conduction and valence bands for Si-nc are in-

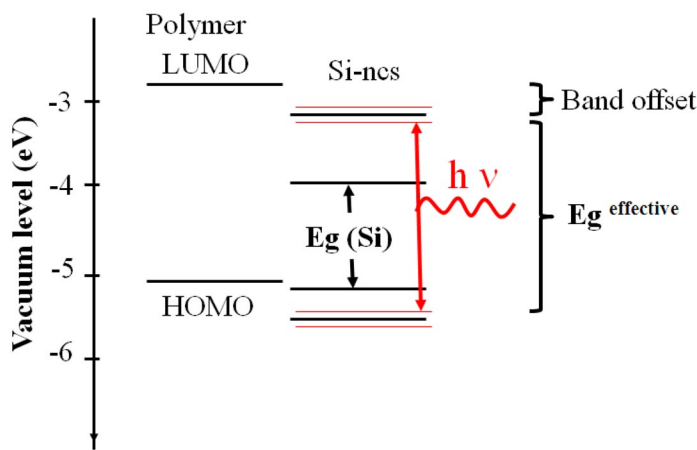


**Fig. 8** Proposed energy level diagram of Si-NCs conjugated polymer-based blends. Value for ionization energy of Si-NCs is taken from the PL measurements with respect to the characteristics of the bulk Si. Levels of HOMOs and LUMOs are taken from the literature (see text).

dicated in Fig. 8 by the red color. Although it has been reported for other types of the NCs that this transition is optically forbidden [73] it can, however, be involved in the Dexter energy transfer [69,71]. In eq. 1, the  $P_D(E)$  and  $A_A(E)$  terms involve forbidden transitions, which results in a decrease of the NC's effective gap ( $E_g^{\text{effective}}$ , Fig. 8). Consequently it becomes easier for the excitation energy to find a specific lower exciton state in Si-NCs. This leads to a red-shift in PL spectra of the blended Si-NCs (Fig. 7). As the degree of the PL emission overlapping is smaller for P3HT polymer, the value of  $R_{\text{ET}}$  integral is smaller as well. After exciton transfer, the radiative recombination is possible in Si-NCs with larger diameter (i.e., lower-energy bandgap) at less efficient emission rates.

Furthermore, in our studied Si-NCs with sizes of 3 nm on average and wide optical gap  $\sim$ 2 eV, both the hole and electrons are strongly spatially confined. Therefore, the dielectric constant of the NCs has to be considered in strong confinement regime as well [72]. If the dielectric constant is strongly confined, then the distance from the polymer to the NC is reduced. In fact, the dielectric constant reduces the screening effect. This leads to an increase in the Förster transfer time from the polymer to NC. An effective interaction center of the dipole in the NC increases as a function of the size [69]. However, in the case of weak confinement (Si-NC diameter  $> 8$  nm), since the exciton can move around the NC, one can argue that the energy transfer between the NCs and the P3HT polymer can be described both terms: (i) by phase-coherent strong coupling and (ii) phase-incoherent weak coupling through the resonant dipole–dipole interaction [74–77]. Or, in other words, the excitation energy is transferred to the larger sized Si-NCs by the Förster-like transfer. If the P3HT polymer-based blend is viewed as an inhomogeneous collection of varying-length chain segments. Then, after a photon excites a chain segment exciton executes a random walk through the density of states via the Förster energy transfer. The excitation energy transfer duration is, until it interacts with the larger-sized NC ( $> 8$  nm) and the Förster mechanism cannot be completely ruled out. However, in our case, the temperature-dependent PL indicates that most of the exciton transfer goes into the Si-NCs with an optical bandgap around 720 nm (1.7 eV) corresponding to a size of about  $\sim$ 4 nm on average. On this scale, the electrons and holes are still confined and the dipole–dipole coupling with the polymer is limited. Therefore, it is assumed that similarly to the Si-NC/MEH-PPV blend, the Dexter-like mechanism plays a major role for the excitation energy transfer in the Si-NC/P3HT blend. The Si-NC/MEH-PPV polymer blend luminescence properties brings to mind many novel optoelectronic applications (e.g., organic light-emitting diode), the red-shifted PL and decreased emission rate from Si-NCs embedded in P3HT polymer are more favorable for construction of the photovoltaic devices. As demonstrated in Fig. 5b, contrary to MEH-PPV polymer, a higher delocalization of the carriers in lamella-like P3HT polymer limits a back recombination of the electrons transferred in Si-NCs and holes in the polymer and increases the photocurrent generation.

## CONCLUSIONS

Photoelectric properties of Si-NCs blended with P3HT and MEH-PPV conjugated polymer were investigated. An improvement in a photo-conductivity response is demonstrated when NCs are blended within both the polymers at ambient temperature and atmosphere. The occurrence of interaction between the electronic ground states of Si-NCs and both polymers establishes a bulk heterojunction. An off-set between the polymer work function and NC ionization potential led to a dissociation of the excitons. The electrons are swept into the conduction band of the Si-NC, while the holes are transferred into the polymer. An exciton emission reduction combines with an increase of the transport properties, thus improving the photo-response in the lamella-structured P3HT-based blend. An addition of NCs in both polymers affects the vibrational relaxation and changes the profile of the PL emission of the blend. Dexter mechanism is responsible for the excitation energy transfer to the Si-NCs with a quantum confinement size effect. The excitation-transfer energy from the polymer to a NC leads to a red-shift of the blends PL emission. A decreased energy transfer rate is observed for the P3HT-based blend due to the smaller overlap between the emission spectra with NCs and in addition places it in the low-energy re-

gion. It is assumed that after the Dexter-like energy transfer of the PL band can be attributed mainly to zero-phonon electron-hole recombination in Si-NCs due to a strong enhancement of the quantum confinement effect. It is believed that conjugated polymers blended with Si-NCs with quantum confinement effects have potential for the development of environmentally compatible and low-cost photovoltaic devices.

## ACKNOWLEDGMENT

This work was also partially supported by a NEDO project.

## REFERENCES

1. C. J. Brabec, V. Dyakonov. In *Organic Photovoltaics: Concepts and Realization*, C. J. Brabec, V. Dyakonov, J. Parisi, N. S. Sariciftci (Eds.), Springer-Verlag, Berlin (2003).
2. H. Sirringhaus, P. J. Brown, R. H. Friend, M. M. Nielsen, K. Bechgaard, B. M. W. Langeveld Voss, A. J. H. Spiering, R. A. J. Janssen, E. W. Meijer, P. Herwig, D. M. de Leeuw. *Nature* **401**, 685 (1999).
3. J. Y. Seong, K. S. Chung, S. K. Kwak, Y. H. Kim, D. G. Moon, J. I. Han, W. K. Kim. *J. Korean Phys. Soc.* **45**, 5914 (2004).
4. W. R. Salaneck, O. Inganäs, B. Themans, J. O. Nilsson, B. Siogren, J.-E. Osterholm, J.-L. Bredas, S. Svensson. *J. Chem. Phys.* **89**, 4613 (1988).
5. Y. Shao, G. Yuan, P. Reche, M. Lecerc. *Polymer* **36**, 2211 (1995).
6. F. Padinger, R. S. Rittber, N. S. Sariciftci. *Adv. Funct. Mater.* **13**, 85 (2003).
7. D. R. Baigent, R. N. Marks, N. C. Greenham, R. H. Friend, S. C. Moratti, A. B. Holmes. *Appl. Phys. Lett.* **65**, 2636 (1994).
8. V. Bulovic, P. Tian, P. E. Burrows, M. R. Gokhale, S. R. Forrest, M. E. Thompson. *Appl. Phys. Lett.* **70**, 2954 (1997).
9. D. Y. Kim, S. K. Lee, J. L. Kim, H. Lee, H. N. Cho, S. I. Hong, C. Y. Kim. *Synth. Met.* **121**, 1707 (2001).
10. X. Yang, J. Loos, S. C. Veenstra, W. J. H. Verhees, M. M. Wienk, J. M. Kroon, M. A. J. Michels, R. A. J. Janssen. *Nano Lett.* **5**, 579 (2005).
11. P. Peumans, S. R. Forrest. *Appl. Phys. Lett.* **79**, 126 (2001).
12. M. M. Wienk, J. M. Kroon, W. J. H. Verhees, J. Knol, J. C. Hummelen, P. A. van Hal, R. A. J. Janssen. *Angew. Chem., Int. Ed.* **42**, 3371 (2003).
13. C. J. Brabec. *Sol. Energy Mater. Sol. Cells* **83**, 273 (2004).
14. V. L. Colvin, M. C. Schlamp, A. P. Alivisatos. *Nature* **370**, 354 (1994).
15. N. Tessler, V. Medvedev, M. Kazes, S. Kan, U. Banin. *Science* **295**, 1506 (2002).
16. L. Bakueva, S. Musikhin, M. A. Hines, T. W. F. Chang, M. Tzolov, G. D. Scholes, E. H. Sargent. *Appl. Phys. Lett.* **82**, 2895 (2003).
17. A. A. R. Neves, A. Camposeo, R. Cingolani, D. Pisignano. *Adv. Funct. Mater.* **18**, 751 (2008).
18. C. J. Brabec, N. S. Sariciftci, J. C. Hummelen. *Adv. Funct. Mater.* **11**, 15 (2001).
19. S. A. Choulis, J. Nelson, Y. Kim, D. Poplavskyy, T. Kreouzis, J. R. Durrant, D. D. C. Bradley. *Appl. Phys. Lett* **83**, 3812 (2003).
20. F. W. Wise. *Acc. Chem. Res.* **33**, 773 (2003).
21. K. Sill, T. J. Emrick. *J. Am. Chem. Soc.* **126**, 11322 (2004).
22. A. J. Mozer, P. Denk, M. C. Scharber, H. Neugebauer, N. S. Sariciftci. *J. Phys. Chem. B* **108**, 5235 (2004).
23. C. Winder, N. S. Sariciftci. *J. Mater. Chem.* **14**, 1077 (2004).
24. T. Hasobe, Y. Kashiwagi, M. A. Absalom, J. Sly, K. Hosomizu, M. J. Crossley, H. Imahori, P. V. Kamat, S. Fukuzumi. *Adv. Mater.* **16**, 975 (2004).

25. M. A. Hines, G. D. Scholes. *Adv. Mater.* **15**, 1844 (2003).
26. J. Brabec, N. S. Sariciftci, J. C. Hummelen. *Adv. Funct. Mater.* **11**, 15 (2004).
27. V. Švrček, H. Fujiwara, M. Kondo. *Appl. Phys. Lett.* **92**, 143301 (2008).
28. L. Yi, R. Scholz, M. Zacharias. *J. Photoluminescence* **122–123**, 750 (2007).
29. M. C. Beard, K. P. Knutsen, P. Yu, J. M. Luther, Q. Song, W. K. Metzger, R. J. Ellingson, A. J. Nozik. *Nano Lett.* **7**, 2506 (2007).
30. L. Mangolini, D. Jurbergs, E. Rogojina, U. Kortshagen. *J. Photoluminescence* **121**, 327 (2006).
31. V. Švrček, A. Slaoui, J.-C. Muller. *J. Appl. Phys.* **95**, 3158 (2004).
32. J. Valenta, A. Fucikova, F. Vacha, F. Adamec, J. Humpolickova, M. Hof, I. Pelant, K. Kusová, K. Dohnalova, J. Linnros. *Adv. Funct. Mater.* **18**, 2666 (2008).
33. Y. Kanemitsu, H. Uto, Y. Masumoto, T. Matsumoto, T. Futagi, H. Mimura. *Phys. Rev. B* **48**, 2827 (1993).
34. G. Amato, M. Rosenbauer. *Structural and Optical Properties of Porous Silicon Nanostructures*, G. Amato, C. Delerue, H.-J. von Bardeleben (Eds.), p. 3, Gordon and Breach, London (1997).
35. P. M. Fauchet. *Light Emission in Silicon: From Physics to Devices, Semiconductors and Semimetals*, Vol. 49, D. J. Lockwood (Ed.), Chap. 6, p. 205, Academic Press, San Diego (1998).
36. D. Kovalev, H. Heckler, G. Polisski, F. Koch. *Phys. Status Solidi A* **215**, 871 (1999).
37. D. Kovalev, H. Heckler, M. Ben-Chorin, G. Polisski, M. Schwartzkopff, F. Koch. *Phys. Rev. Lett.* **81** 2803 (1998).
38. M. V. Wolkin, J. Jorne, P. M. Fauchet, G. Allan, C. Delerue. *Phys. Rev. Lett.* **82**, 197 (1999).
39. A. G. Cullis, L. T. Canham, P. D. J. Calcott. *Phys. Rev. Lett.* **82**, 909 (1997).
40. G. Belomoin, J. Therrien, M. Nayfeh. *Appl. Phys. Lett.* **77**, 779 (2000).
41. S. Komuro, T. Kato, T. Morikawa, P. O'Keeffe, Y. Aoyagi. *J. Appl. Phys.* **80**, 1749 (1996).
42. J. D. Holmes, K. J. Ziegler, R. Ch. Doty, L. E. Pell, K. P. Johnston, B. A. Korgel. *J. Am. Chem. Soc.* **123**, 3743 (2001).
43. Y. Shi, J. Lui, Y. Yang. *J. Appl. Phys.* **87**, 4254 (2000).
44. S. Natarajan, S. H. Kim. *Chem. Commun.* **729**, 15 (2006).
45. H. Becker, S. E. Burns, R. H. Friend. *Phys. Rev. B* **56**, 1893 (1997).
46. R. Kersting, U. Lemmer, R. F. Marht, K. Leo, H. Kurz, H. Bassler, E. O. Gobel. *Phys. Rev. Lett.* **70**, 3820 (1993).
47. A. Zen, J. Pflaum, S. Hirschmann, W. Zhuang, F. Jaiser, U. Asawapirom, J. P. Rabe, U. Scherf, D. Neher. *Adv. Funct. Mater.* **14**, 757 (2004).
48. Y. Kim, S. A. Choulis, J. Nelson, D. D. C. Bradley, S. Cook, J. R. Durrant. *Appl. Phys. Lett.* **86**, 63502 (2005).
49. N. Greenham, X. Peng, A. Alivisatos. *Phys. Rev. B* **54**, 17628 (1996).
50. S. Guha, G. Hendershot, D. Peebles, P. Steiner, F. Kolowski, W. Lang. *Appl. Phys. Lett.* **64**, 613 (1994).
51. M. M. Mandoc, W. Veurman, J. Sweelssen, M. M. Koetse, P. W. M. Blom. *Appl. Phys. Lett.* **91**, 073518 (2007).
52. H. Sirringhaus, P. J. Brown, R. H. Friend, M. M. Nielsen, K. Bechgaard, B. M. W. Langeveld-Voss, A. J. H. Spiering, R. A. J. Janssen, E. W. Meijer, P. Herwig, D. M. de Leeuw. *Nature* **401**, 685 (1999).
53. C. Yin, T. Kietzke, D. Neher, H.-H. Horhold. *Appl. Phys. Lett.* **90**, 092117 (2007).
54. Y. Kim, S. Cook, S. Tuladhar, S. Choulis, J. Nelson, J. Durrant, D. Bradley, M. Giles, I. McCulloch, C. Ha, M. Ree. *Nat. Mater.* **5**, 197 (2006).
55. P. A. C. Quist, T. J. Savenije, M. M. Koetse, S. C. Veenstra, J. M. Kroon, L. D. A. Siebbeles. *Adv. Funct. Mater.* **15**, 469 (2005).
56. P. J. Brown, H. Sirringhaus, M. Harrison, M. Shkunov, R. H. Friend. *Phys. Rev. B* **63**, 125204 (2001).

57. X. Yang, J. Loos, S. C. Veenstra, W. J. H. Verhees, M. M. Wienk, J. M. Kroon, M. A. J. Michels, R. A. J. Janssen. *Nano Lett.* **5**, 579 (2005).
58. K. Pichler, D. A. Halliday, D. D. C. Bradley, P. L. Burn, R. H. Friend, A. B. Holmes. *J. Phys.: Condens. Matter* **5**, 7155 (1993).
59. J. Yu, M. Hayashi, S. H. Lin, K. K. Liang, J. H. Hsu, W. S. Fann, C. Chao, K. Chung, S. Chen. *Synth. Met.* **82**, 159 (1996).
60. M. L. Brongersma, A. Polman, K. S. Min, E. Boer, T. Tambo, H. A. Atwater. *Appl. Phys. Lett.* **72**, 2577 (1998).
61. V. Švrček, H. Fujiwara, M. Kondo. *Sol. Energy Mater. Sol. Cells* **93**, 774 (2009).
62. D. S. Ginger, N. C. Greenham. *Synth. Met.* **124**, 117 (2001).
63. Th. Förster. *Ann. Phys. (N.Y.)* **2**, 55 (1948).
64. D. L. Andrews, A. A. Demidov. *Resonance Energy Transfer*, John Wiley, Chichester (1999).
65. T. Förster. *Discuss. Faraday Soc.* **27**, 7 (1959).
66. T. W. F. Chang, S. Musikhin, L. Bakueva, L. Levina, M. A. Hines, P. W. Cyr, E. H. Sargent. *Appl. Phys. Lett.* **84**, 4295 (2004).
67. J. H. Warner, A. A. R. Watt, E. Thomsen, N. Heckenberg, P. Meredith, H. Rubinsztein-Dunlop. *J. Phys. Chem. B* **109**, 9001 (2005).
68. D. M. Basko, V. M. Agranovich, F. Bassani, G. C. La Rocca. *Eur. Phys. J. B* **8**, 353 (1999).
69. D. L. Dexter. *J. Chem. Phys.* **21**, 836 (1953).
70. L. Nayak, M. K. Raval, B. Biswal, U. C. Biswal. *Photochem. Photobiol. Sci.* **1**, 629 (2002).
71. A. Monguzzi, R. Tubino, F. Meinardi. *Phys. Rev. B* **77**, 155122 (2008).
72. A. D. Andreev, A. A. Lipovskii. *Phys. Rev. B* **59**, 15402 (1999).
73. Y. Kang, F. W. Wise. *J. Opt. Soc. Am. B* **14**, 1632 (1997).
74. V. M. Agranovich, M. D. Galanin. *Electronic Excitation Energy Transfer in Condensed Matter*, North Holland, Amsterdam (1982).
75. M. Achermann, M. A. Petruska, S. Kos, D. L. Smith, D. D. Koleske. *Nature* **429**, 642 (2004).
76. C. R. Kagan, C. B. Murray, M. Nirmal, M. G. Bawendi. *Phys. Rev. Lett.* **76**, 1517 (1996).
77. T. Franzl, D. S. Koktysh, T. A. Klar, A. L. Rogach, J. Feldmann. *Appl. Phys. Lett.* **84**, 2904 (2004).